

Observations of Radiation-Dominated Rapid Cooling of Structures Based on Carbon Nanotubes and Graphene

Faezeh Mohammadbeigi, Lorne Whitehead,* Ranjith Divigalpitiya, and Alireza Nojeh*

It is often desirable to cause rapid thermal cycles in isolated systems, and it is convenient to do so by means of radiant heating and cooling. In principle, the rate of heating is arbitrarily increased simply by applying sufficient irradiance. This is not true for cooling, wherein the radiant emittance of a surface is determined by its emissivity and temperature. In an optically thin structure, the cooling rate is determined by the ratio of the material's emissivity to its specific heat, a factor that is expected to be greater in materials with a short characteristic absorption length, such as graphite. Herein, several forms of carbon-based nanostructures, which have very short thermal radiation attenuation lengths, and are very robust and can withstand the high temperatures required for substantial Planckian thermal radiant emittance, are examined. Rapid cooling times ranging from about 100 μs to 1 ms are observed in structures cooling from a typical high temperature of 1500 K to a low of roughly half that value. Such rapid extreme thermal cycling of isolated materials provides new opportunities, for both research and potentially practical applications.

of rapid temporal variations of temperature is also important, as evidenced by the existence of high-speed infrared cameras. However, in such cases, often the thermal radiation itself is not the primary energy loss mechanism underpinning the temperature changes, but is merely the signal that communicates those changes to a detector. Indeed, in many everyday scenarios, other mechanisms including heat conduction or mass transfer are the dominant energy exchange pathways because radiation is relatively weak because of the low temperature of the application and/or the low emissivity of the materials involved. For example, the gas in an internal combustion engine has quite low emissivity, so the only rapid way to remove the waste heat is by expelling the still-hot gas after each power stroke. On the contrary, as long as there is substantial emissivity, at sufficiently high

1. Introduction

Thermal radiation or black/gray body radiation is a ubiquitous form of energy and information exchange. From incandescent lamps and heaters to pyrometers, thermal cameras, motion sensors, and night vision goggles, to thermophotovoltaic energy converters, many applications depend on the emission and/or collection of thermal radiation. Most of these involve either steady-state operation or slow temporal variations. The study

temperature radiation becomes a major energy loss mechanism, if not the dominant one, potentially enabling very rapid temperature change. The temperature significantly affects the rate of change because of the T^4 relationship depicted in the Stefan–Boltzmann law (where T is the absolute temperature of the thermal emitter). For instance, in an incandescent lamp, where the filament is typically heated to about 2750 K, the light emission appears to stop almost instantly when the heating is switched off (although that is in reality a fairly slow process, with a characteristic time on the order of 100 ms, in comparison to the situations explored in the current work).

Overall, historically, thermal radiation has not been used as a means of changing temperature rapidly. However, this situation could change if a light-emitting structure can have, to a sufficient degree, three properties: an ability to withstand the high operating temperature needed for a sufficiently rapid response, a sufficiently high emissivity for black body radiation at that operating temperature, and a sufficiently low specific heat per unit emitting area. In addition, given that rapid temperature changes can lead to great thermal stress and also the fact that many applications involve mechanical movements and deformations of the material, a high mechanical strength, be it tensile or compressive, is required. An example application is a recently proposed heat engine based on the rapid radiative heating and cooling of a highly absorptive gaseous suspension.^[1]


Carbon is a relatively light element that comes in forms that have relatively low specific heat and are strongly absorptive (and therefore emissive) over a broad spectral range. These forms are also relatively strong and can withstand quite high temperatures.

Dr. F. Mohammadbeigi, Prof. A. Nojeh
Quantum Matter Institute
University of British Columbia
Vancouver, British Columbia V6T 1Z4, Canada
E-mail: alireza.nojeh@ubc.ca

Prof. L. Whitehead
Department of Physics and Astronomy
University of British Columbia
Vancouver, British Columbia V6T 1Z1, Canada
E-mail: lorne.whitehead@ubc.ca

Dr. R. Divigalpitiya
3M Canada Company
1840 Oxford Street East, London, Ontario N5V 3R6, Canada

Prof. A. Nojeh
Department of Electrical and Computer Engineering
University of British Columbia
Vancouver, British Columbia V6T 1Z4, Canada

 The ORCID identification number(s) for the author(s) of this article can be found under <https://doi.org/10.1002/adem.201901315>.

DOI: 10.1002/adem.201901315

For example, even a single layer of graphene, an atomically thin material, absorbs 2.3% of incident light, and carbon nanotube (CNT) forests are known as the darkest synthesized material and have been shown to localize optically induced heat and dissipate it largely through reradiation.^[2] There has been growing interest in nanocarbon-based emitters and absorbers of thermal radiation. Examples include graphene-based optical detectors using various physical mechanisms^[3] such as bolometers,^[4] CNT-based incandescent sources integrated with waveguides,^[5] graphene-based high efficiency solar water desalination,^[6] exfoliated graphite composite structures used for steam generation with solar radiation,^[7] and nanodiamond powder, multiwall CNT, and carbon black being used as high-surface-emissivity coatings on aluminum panels to improve heat sinking.^[8] As seen in these examples, the nanoscale features of these carbon materials provide great flexibility for fashioning them into various structures and devices; the rapid radiative cooling property of carbon makes it a unique platform that can enable novel applications such as the previously mentioned heat engine.^[1] Figure 1 shows quantitative insight into this unique combination of properties for nanocarbon, by positioning graphene on a scatter plot of tensile strength versus a simple measure of cooling speed (which is determined by emissivity and heat capacity as described in the caption) estimated for a number of common materials. In addition, as graphene and CNTs are in theory chemically complete structures, they are relatively inert and stable (although defects weaken this stability), making them better suited to use in the form of thin layers or nanowires than, for example, bulk metals.

The study of optical absorption and thermal radiation in carbon and resultant temporal temperature variations thus holds much promise. In the current work, we are concerned with optical heating and radiative cooling of several low-density carbon-based systems: multilayer graphene structures, arrays

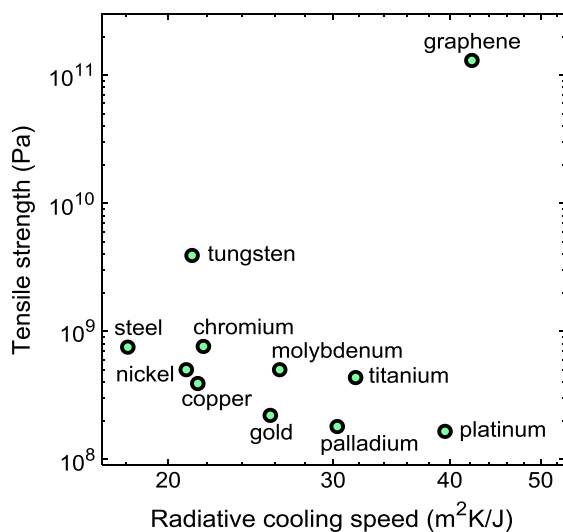


Figure 1. A scatter plot of tensile strength versus relative radiative cooling speed estimated for a number of metals as well as graphene. Relative radiative cooling speed is defined here simply as the ratio of optical absorption per unit thickness of the material, divided by the volumetric specific heat. This speed describes the cooling of free-standing optically thin films. The values shown are based on room temperature data.

of vertically aligned CNTs (CNT forests), and collections of graphitic sheets rolled into structures with diameters of hundreds of micrometers to millimeters (henceforth termed scrolls). The time scales of interest range from hundreds of microseconds to tens of milliseconds, which are relevant to macroscale applications such as radiative heat engines.^[1] We also study the effect of an inert gaseous environment on these dynamics, and the pressure range in which the heating and cooling remain essentially unaffected by the gas and are instead dominated by optical properties.

Given the rich literature on the heating and cooling dynamics of carbon-based materials over a very wide range of time scales, to place this work in context, we start by presenting a brief literature survey spanning these time scales before discussing our experiments and results.

2. Overview of the Dynamics of Heating and Cooling in Conductive Carbon-Based Materials

Here, we survey the dynamics of heating and cooling in carbon, which are complex because at different time scales different phenomena predominate. We consider the range from femtoseconds to milliseconds.

When mobile electrons in graphene or graphite are excited by intense incoming light, they thermalize with each other within tens of femtoseconds and form a hot-electron bath at a temperature that can be substantially higher than that of the lattice because of weak screening and strong electron–electron interactions in the material.^[9–11] Remarkably, electronic temperatures as high as 5500 K have been reported.^[11] Electron energy loss to phonons takes picoseconds, and for the electrons to reach equilibrium with both optical phonons and acoustic phonons, it takes hundreds of picoseconds to nanoseconds.^[12] (In these relaxation processes, radiative loss plays a negligible role.) The rapid optical response of graphene and CNTs has been exploited to fabricate composites based on them for use as saturable absorbers in ultrafast lasers.^[13,14]

Heat transfer from nanocarbon materials to adjacent structures can also be very fast. For example, single-walled CNTs wrapped in sodium dodecyl sulfate (SDS) and illuminated with subpicosecond laser pulses have been observed to lose the heat to the SDS micelles with a time constant of 45 ps.^[15] On-chip, electrically driven black body emitters have been demonstrated based on graphene, with a response time of 100 ps attributed to thermal transport through the surface polar phonons of the substrate.^[16] Electrically driven CNT black body emitters have also been shown, with the fast, 140 ps pulsed operation explained by the small heat capacity of the nanotube film and its high heat dissipation to the substrate.^[17] Similar time scales have also been observed in detectors, for example, subnanosecond response in a hot-electron bolometer based on bilayer graphene.^[18] A suspended powder of multiwall CNTs, heated with a pulsed laser, has been observed to cool down over several tens of nanoseconds, with the mechanism purported to be axial heat diffusion from the surface toward the core of the CNTs.^[19] Illumination of a multiwall CNT forest with a pulsed laser (with a pulse width of several nanoseconds) has led to a temperature rise to 700 K and subsequent decay time of several microseconds to several tens of

microseconds depending on the height of the forest, with the effect explained as arising from conductive cooling.^[20] Chemical vapor-deposited graphene devices (with dimensions of several hundred micrometers) have been made into thermal midinfrared light emitters, and responded to 5 μ s electrical pulses (although the emission intensity at this drive frequency was about two orders of magnitude weaker than when the device was driven at 1 kHz), with the heat dissipation speculated to be primarily conduction to the substrate;^[21] a subsequent study has confirmed that the dominant heat conduction pathway was indeed from the graphene layer to the substrate and that the thermal resistance between the two determined the modulation characteristics.^[22] Single-walled CNT films heated using 1 ps laser pulses have been observed to exhibit a cooling time of 160 μ s, again attributed primarily to conduction.^[23] Cooling of electrically heated CNT yarns in a fraction of a millisecond has been observed, and it was suggested that both conduction and radiation contributed to the cooling.^[24] Another study has reported the cooling of electrically heated super-aligned CNT films in about 1 ms, with the response attributed to the ultrasmall heat capacity per unit area and high emissivity of the structure.^[25] In a yet slower case, the thermal diffusivity of a single-walled CNT forest (with a height of a few millimeters) was observed by illuminating its top surface with a pulsed laser and recording the evolution of the temperature at its bottom surface using a fast infrared radiometer,^[26] with the observed delay of several milliseconds being attributed to thermal transport through the forest, suggesting that the heating dynamics of the bottom surface itself must be faster than milliseconds.

A related phenomenon is the cooling behavior of carbon fiber layers on arc electrodes, where conduction through the layer was thought to dominate within the first 100 μ s, possibly with a contribution from radiative transfer during the first 20 μ s, and subsequently conduction through the bulk took place over several tens of milliseconds, leading to significant cooling.^[27]

In the present article, we report on experiments involving three different forms of carbon at temperatures where radiative heat loss appears to be dominant, leading to temperature decay in hundreds of microseconds to milliseconds. Note that in the majority of previous works relevant to this temporal range, radiation has not been an important contributor to cooling. The exceptions have been where a combination of conductive and radiative cooling has been observed in electrically heated CNT films,^[24,25] with our observations differing from those in three ways: 1) we used a focused laser beam for heating the material far away from its points of contact with the substrate or electrodes, thus minimizing conduction to external heat sinks so as to enable observation of the effect of thermal radiation in isolation; 2) we studied three different carbon systems (including CNTs), which leads to a broad and comparative perspective; and 3) we investigated the effect not only in vacuum but also in an inert gas environment over the several orders of magnitude of pressure within which radiation remained the dominant cooling mechanism.

3. Sample Fabrication and Experiments

We fabricated and characterized three types of structures, the schematics of which can be seen in **Figure 2a–c**. The first consisted of multilayer graphene sheets (between 30 and 60 layers in thickness) suspended over holes (with diameters in the range of 0.5–2 mm) etched in silicon using deep reactive ion etching. The graphene sheets were grown using chemical vapor deposition on nickel foil by Graphene Platform Corp., Japan. Poly(methyl methacrylate) (PMMA) was then coated on the graphene grown on the front side of the nickel substrate. Subsequently, the back side graphene and nickel substrate were removed by reactive ion etching and nickel etchant, respectively. Then the PMMA-coated graphene was transferred onto the silicon substrate to cover the holes, and the PMMA etched away using acetone. The second

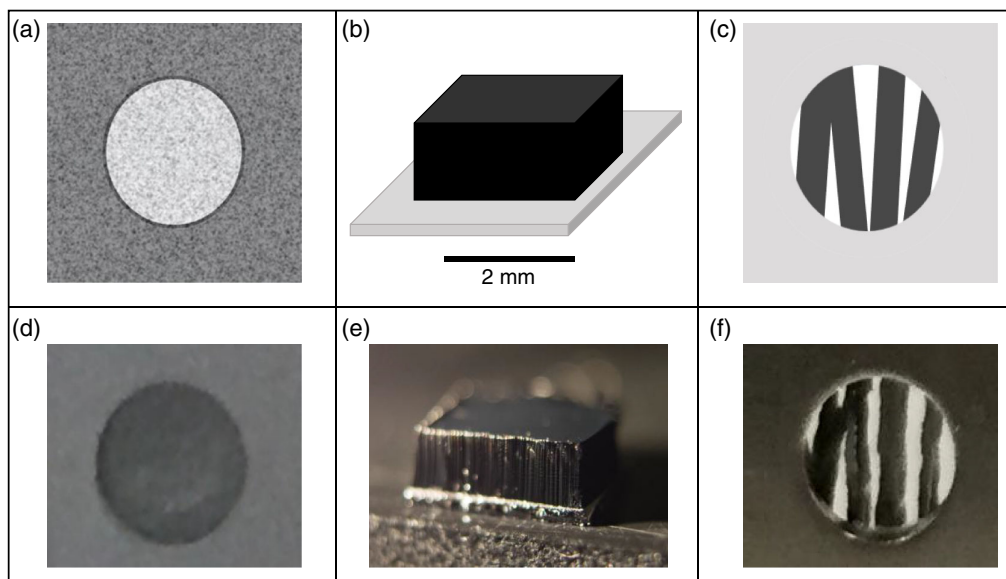


Figure 2. a–c) Schematic representations of the suspended graphene, CNT forest, and scrolls, respectively. d–f) Photos of the three structures. The scale bar shown applies to all panels. In parts (c) and (f), the GLC scrolls appear as dark regions in the hole, and the light regions are empty space.

type of structure was multiwall CNT forests that we grew on silicon substrates using ethylene-based chemical vapor deposition with an iron layer (≈ 1 nm in thickness) as catalyst deposited over an alumina layer (≈ 10 nm in thickness). The third type consisted of collections of randomly oriented graphitic scrolls (with diameters in the range of 0.5–2 mm—here we show results for ≈ 0.5 mm scrolls). The details of the preparation of scrolls are described elsewhere.^[28] Briefly, a proprietary 3M coating technology, called graphene-like carbon (GLC) coating, was used. First, a 3M Scotch tape was attached to a flat glass plate, and a sufficiently thick coating of GLC was deposited onto the release side (opposite to the adhesive side) of this tape. Then the tape was peeled off slowly at a constant angle, and the GLC coating separated from the release side of the tape and curled inward to form scrolls. By varying the peeling angle, the diameter of the scrolls can be controlled, and the width of the Scotch tape determines the width of the scrolls. Figure 2d–f shows representative photos of the three types of structures.

We performed the experiments in a vacuum chamber pumped to a base pressure of 2.5×10^{-6} mbar with a turbomolecular pump; each experiment started at this pressure. A leak valve allowed us to subsequently introduce argon (with a purity of 99.9%) to control the pressure. For pressures between 2.5×10^{-6} and 1×10^{-5} mbar, we kept the turbomolecular pump on. For higher pressures until 1×10^{-1} mbar, we turned off the turbomolecular pump but kept its backing scroll roughing pump on. Pressure control in those ranges was thus achieved using a steady-state flow. For yet higher pressures, up to a few millibars, we turned off the scroll pump as well and achieved the desired pressure with zero flow in steady state. The pressure was stable for more than 5 min, which was much longer than needed for the experiments. The structure under characterization was placed behind a Lesker VPZL-800 Kodial glass viewport, and a continuous-wave laser beam with a wavelength of 532 nm and a power in the range of 30–90 mW was focused to a ≈ 65 μm -diameter spot on the sample through the viewport. A mechanical chopper was used to generate pulses with a duty cycle of 50% typically at 400 Hz, corresponding to a pulse width of 1.25 ms (and, given the laser spot size of 70 μm at the chopper plane, a laser cutoff time of 0.7 μs). The temperature of the illuminated spot (both with and without chopping of the laser light) was measured using a disappearing-filament pyrometer. For the different structures, emissivity values of 0.8–1 were assumed for the purpose of pyrometry based on known properties of the respective materials. The pyrometer relies on the operator to use a control knob to make a hot filament “disappear” against the incandescent glow of the region whose temperature is being measured. Given the dependence of this measurement technique on the operator’s visual judgment and also the uncertainties involved in emissivity values, our temperature measurements had an uncertainty of ± 50 K, which is sufficiently low for the current study. A portion of the thermal radiation from the hot spot was collected using a biconvex lens with a numerical aperture of 0.3 and focused onto an InGaAs photodiode with a nominal spectral sensitivity range of ≈ 800 –1700 nm and connected to a transimpedance amplifier, the output of which was measured and recorded using an oscilloscope. A NoIR Laser ARG optical filter placed in front of the photodiode was used to block stray

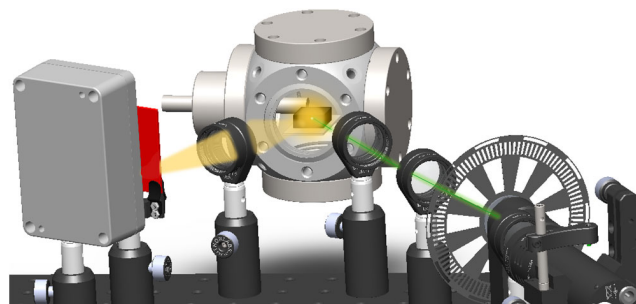


Figure 3. Schematic of the experimental apparatus. The laser beam (green) starts at the bottom right, passes through the chopper wheel, and is focused onto the sample inside the vacuum chamber. The thermal radiation (diverging yellow beam) is focused onto the photodiode inside the box on the left.

light due to reflections of the green laser. A schematic of the experimental apparatus is shown in **Figure 3**.

4. Results and Discussion

Figure 4a shows the normalized voltage signal measured by the oscilloscope during a typical cooling process. We use this signal to extract the time evolution of temperature (for simplicity, we assume an approximately uniformly heated spot). This signal is due to the thermal radiation received by the photodiode and is given by

$$v_N(t) = V_0 \int_{\lambda_1}^{\lambda_2} D(\lambda) B_{T(t)}(\lambda) d\lambda \quad (1)$$

where V_0 is a normalization constant encompassing factors such as the transimpedance gain, the area of the hot spot, the signal collection solid angle, and the emissivity of the sample (which we take to be constant over the spectral range involved, as we further justify later); $D(\lambda)$ is the combined spectral response of the photodiode and the optical path (including the viewport, lens, and filter); and $B_{T(t)}(\lambda)$ is the spectral radiance of a black body at temperature T , given by

$$B_{T(t)}(\lambda) = \frac{2hc^2}{\lambda^5} \frac{1}{e^{\frac{hc}{\lambda T(t)}} - 1} \quad (2)$$

where h is the Planck constant, k is the Boltzmann constant, and c is the speed of light. The integration limits λ_1 and λ_2 define the wavelength range beyond which the photodiode has negligible response. At each point in time, we numerically vary the value of temperature until the integral in Equation (1) matches the measured voltage signal. This requires knowledge of the normalization constant, the estimation of which requires additional information (peak temperature). This information is given by the disappearing-filament pyrometer, which works based on a visual comparison, in the 650–670 nm spectral range (defined by an internal filter), of the intensity of the radiation from the region of interest with that of a heated filament with known temperature. In this case, the chopped signal is viewed, with a 50% duty cycle, at the chopping frequency of 400 Hz. The resultant

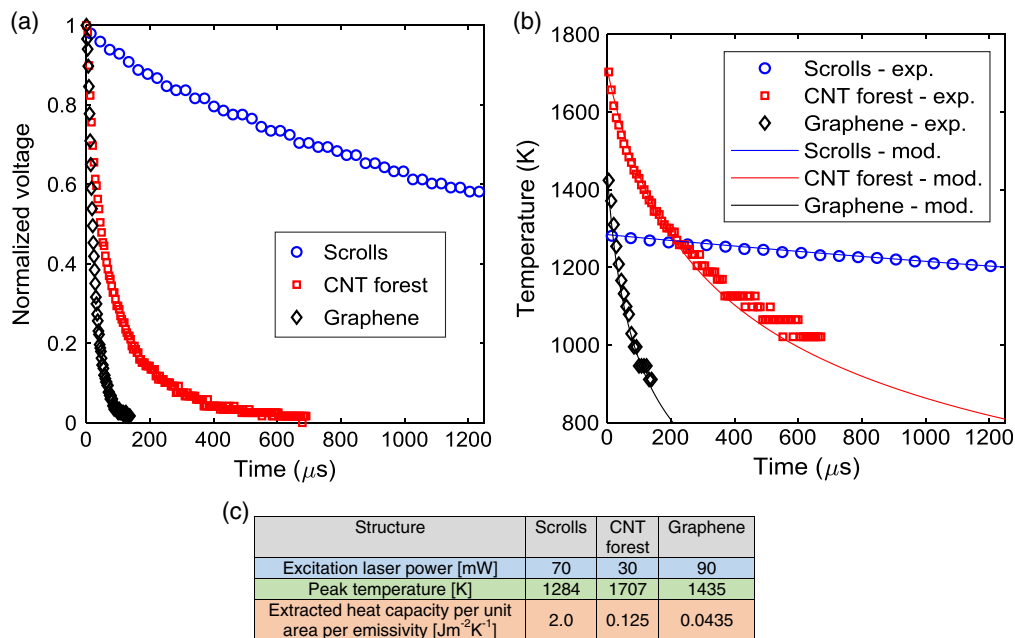


Figure 4. a) Normalized measured voltage signals (due to thermal radiation) from the three carbon-based nanostructures during cooling. b) Derived temperatures during cooling (determined from the measured voltage signals) and corresponding modeled values. c) Input power used and peak temperature achieved for each structure, as well as the value of heat capacity per unit area per emissivity obtained by fitting the temperature response as shown in part (b).

flicker is not visible so the time-averaged light intensity is what determines the pyrometer reading. We interpreted these readings by using the time-average of an equation similar to Equation (1) to determine the peak temperature. Based on all of this information, the temperatures as a function of time during the cooling cycle were determined for the three materials. These are shown in Figure 4b.

The three materials exhibit different cooling rates presumably due to differences in emissivity and heat capacity (although possible contributions from thermal conduction cannot be fully dismissed). To gain a quantitative understanding, we modeled the radiative cooling based on the Stefan–Boltzmann law by numerically solving

$$C \frac{dT}{dt} = -\alpha\epsilon\sigma(T^4 - T_{\text{amb}}^4) \quad (3)$$

where C is the heat capacity per unit area, ϵ is the emissivity, σ is the Stefan–Boltzmann constant, and T_{amb} is the ambient temperature (taken to be 300 K), using a finite-difference approach in the time domain. α is a factor which is 1 if radiation happens only from the front surface (corresponding to the cases of the CNT forest and the scrolls, both of which are millimeters thick) and 2 if it happens from both sides (corresponding to the graphene case where the structure is only tens of nanometers in thickness). Whether the aforementioned radiation-dominated cooling model (neglecting the role of conduction) adequately describes our results is addressed later by considering the quality of the radiation-based fit to the experimental data.

We extract the ratio of heat capacity per unit area to emissivity, c/ϵ , for each material by fitting this calculated temperature

(solid lines in Figure 4b) to the temperature extracted from the measured voltage signal (markers in Figure 4b); the results are shown in Figure 4c. The value of emissivity for graphene is 0.023 per layer for photon energies greater than 0.5 eV (which covers our detection range),^[29] and for the CNT forest, which is an almost perfect black body, it is ≈ 1 ; for the scrolls, it is expected to be lower given their grayish appearance. The specific heat of graphene is $\approx 1.9 \text{ Jg}^{-1} \text{ K}^{-1}$ at elevated temperatures.^[30] Assuming an effective graphene layer thickness of 3.4 Å, this leads to a heat capacity per unit area of $\approx 1.5 \times 10^{-3} \text{ Jm}^{-2} \text{ K}^{-1}$, yielding $c/\epsilon = 0.065 \text{ Jm}^{-2} \text{ K}^{-1}$. The extracted value of $0.0435 \text{ Jm}^{-2} \text{ K}^{-1}$ (Figure 4c) is in good order-of-magnitude agreement with this estimate. (Note that the number of graphene layers in the structure is inconsequential to first order because optical absorption and heat capacity both scale linearly with the number of layers in this range of thickness.) For the CNT forest, the extracted value is $0.125 \text{ Jm}^{-2} \text{ K}^{-1}$. The fact that this is also approximately of the same order of magnitude as the value for graphene is not surprising. Although knowledge of the depth of the heated region is required to estimate the relevant value of heat capacity per unit area of the illuminated spot for the CNT forest, for a simple evaluation, one may expect that, whether in the form of a multilayer graphene structure or a CNT forest, a similar total number of carbon atoms is required for a given amount of optical absorption. Thus, the ratio of emissivity per heat capacity per unit area is expected to be comparable for the CNT forest and the graphene structure. A major difference between the two materials is thus the fact that the thin graphene layer radiates from both sides, whereas the thick CNT forest does so only from the front surface, leading to half the amount of radiation and correspondingly slower cooling for the latter.

For the scrolls, a significantly slower response was measured as shown in Figure 4a,b, leading to an extracted c/ϵ value of $2.0 \text{ J m}^{-2} \text{ K}^{-1}$. We also note that both graphene and CNT forests have a cooling response time in the hundreds of microseconds; for the scrolls, the value is in the milliseconds. These significant differences between the scrolls and the other two samples (graphene and CNT forest) are not surprising, given the former's significantly different structure and bulky nature, where likely a much larger volume of the material is involved in the heating and cooling. Indeed, the above c/ϵ value for the scrolls appears to be approaching that of graphite, which we estimate at $3.2 \text{ J m}^{-2} \text{ K}^{-1}$ based on data available in the literature.^[30–32]

The aforementioned analysis leads to reasonable values for c/ϵ , lending further credibility to our aim for radiation to be the dominant cooling mechanism, with the contribution from conduction to surroundings being, by comparison, negligible. Nonetheless, one might argue that graphene and CNTs may both have higher thermal conductivity than the scrolls, and that the faster cooling rate for those structures is partially due to conduction. While the good quality of the fit of our radiation-only model to the experimental results largely counters this argument, this possibility is worth further consideration. We note that, due to the differences in dimensionality, the nature of heat conduction in the three structures is very different: in the CNT forest, conduction is highly anisotropic and essentially along one direction only (along the direction of the nanotubes, which are aligned); in graphene, conduction takes place in two directions (within the plane); and in the scrolls, it is expected to have strong components in all three directions. We have previously presented a detailed modeling study of the effect of dimensionality on heat localization and shown that 1D propagation leads to effective quenching of conduction and thus strong heat confinement and efficient heating.^[33] As a result, the hot spot in the CNT forest is essentially confined to the illuminated region^[33] (consistent with the higher temperature of the CNT forest compared with the other structures for significantly lower amounts of excitation laser power—see Figure 4c). On the contrary, in the case of graphene and scrolls, due to more facile conduction, we have observed that the heat spreads to a substantially larger spot than the illuminated region. Based on this argument, if conduction to surroundings played a major role in cooling in the present experiments, one would expect a faster response from the scrolls than from the CNT forest, which is clearly not the case. (However, it is conceivable that a small contribution from conduction could partially explain the faster response of graphene compared with the CNT forest.)

It is worth emphasizing that our arguments only apply to the high-temperature range in discussion here, where the T^4 form of thermal radiation has made it dominant. An important issue to consider is that thermal conductivity could depend on temperature, with a characteristic $1/T$ or even possibly $1/T^2$ dependence that would make it much smaller in the high-temperature range compared with temperatures of only a few hundred degrees.^[34] Such a rapid drop in conductivity at high temperatures may be partially responsible for the strong thermal confinement we have previously observed in CNT forests.^[33] Therefore, at lower temperatures, conduction may play a significant and eventually even dominant role, given the high intrinsic thermal conductivity of graphene and CNTs.

Thus, from a practical standpoint, the overall conclusion of our observations and the discussion presented earlier is that, in all the forms studied, nanocarbon at temperatures greater than 1000 K has a cooling time of milliseconds or less, and this is predominantly attributable to thermal radiation. (For the scrolls, we have verified the total cooling time by using lower chopping frequencies—not shown.)

We next studied the effect of an inert gaseous environment, in this case Ar. Figure 5 shows that the temperature due to continuous illumination stays relatively constant up to pressures of about 0.1 mbar. At higher pressures, a drop in temperature is observed, consistent with transport of heat into the gas: at 0.1 mbar and 300 K, the impact rate of argon atoms on the hot surface can be estimated to be $8.5 \times 10^{23} \text{ m}^{-2} \text{ s}^{-1}$ and the average energy removed by an argon atom upon impacting a 1800 K surface is about $3 \times 10^{-20} \text{ J}$. For a hot region of several hundred micrometers in diameter, this leads to a cooling power of several tens of mW—a significant fraction of the incident laser power.

We do note an anomaly in the transition region from predominantly radiative to predominately gaseous-conduction cooling, where the temperature appears to slightly increase. We do not yet have an explanation for this observation, but have considered several possibilities. Given the purity level of 99.9% for the Ar gas used and the care we took in purging the system for long enough times before the experiments, the presence of a substantial amount of oxygen to allow combustion is unlikely. Furthermore, combustion is not a plausible explanation for this temperature increase, as in our experiments we observed that the high temperature in this regime could be sustained for at least 10 s. An estimate based on the available heat of combustion per carbon atom and the number of atoms present in the hot region of the graphene layers shows that combustion could account for temperature rise for only a duration of a few hundred milliseconds; therefore, it cannot explain the observed phenomenon

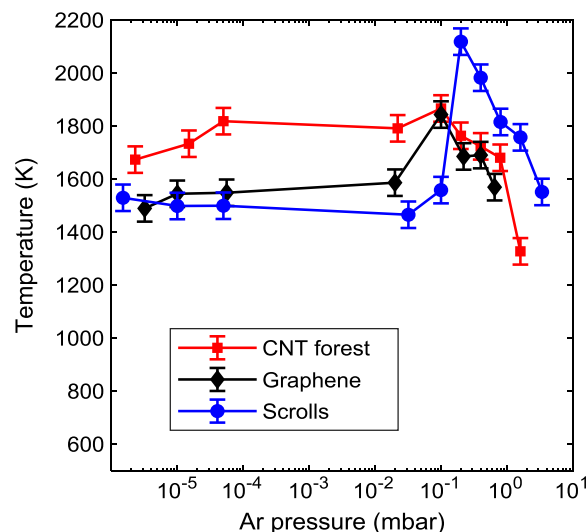


Figure 5. Temperature measured using a pyrometer as a function of pressure in an Ar gas environment for the three structures, showing lack of any significant cooling due to the gas at pressures below 0.1 mbar. The sample is under continuous illumination in these experiments.

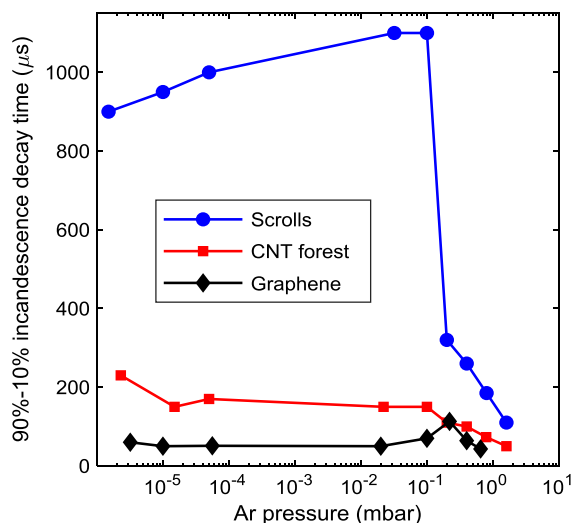


Figure 6. The time that it takes the measured voltage signal to drop from 90% to 10% of its initial value for the three structures, showing lack of any significant cooling due to the gas at pressures below 0.1 mbar.

(although the occurrence of some degree of combustion cannot be entirely ruled out; optical and electron microscopy after the experiments did reveal signs of local damage and, in some cases, puncturing). A more realistic possibility is that, due to interaction with the gas, somehow the optical absorptivity increases. For example, permeation of gas molecules in between the graphene layers might alter the interlayer spacing and thus lead to a different/higher optical absorptivity, leading to higher temperature (and even possible destruction). However, at this point we are not able to put such theories to test and believe that this phenomenon merits a separate and dedicated study in the context of future work.

We finally turn to the effect of gas pressure on cooling time. **Figure 6** shows the time it takes for the measured voltage signal to drop from 90% to 10% of its initial strength. This time remains relatively unaffected up to a pressure of about 0.1 mbar, suggesting that radiation remains the dominant cooling mechanism with negligible contribution from conduction by the gas in that pressure range. This is consistent with the aforementioned observation that the temperature was also unaltered by the presence of gas up to that pressure. At higher pressures, cooling becomes faster.

5. Conclusion

In summary, we have shown that the cooling of various forms of nanocarbon, after being heated to temperatures greater than 1000 K, is dominated by radiation, yielding a temporal response comparable to that expected from radiative cooling. Furthermore, even for macroscopic structures made of these nanomaterials, this radiative cooling is fast, with cooling times of milliseconds or lower. In particular, graphene and CNT forests exhibit a submillisecond response time, consistent with their low heat capacity per unit area relative to their emissivity. Interestingly, radiation remains the dominant energy exchange mechanism

even when the structure is placed in a gaseous environment over a wide range of pressures. In other words, in such mixed environments, the heating and cooling behavior is still primarily determined by the nanocarbon material itself. Together with the mechanical strength and stability of these structures, this rapid macroscale response makes nanocarbon a great candidate for a variety of applications involving fast and large changes of temperature in a contained environment with only optical access and without requiring mass transport, such as novel radiative heat engines and actuators operating at a variety of size scales.

Acknowledgements

The authors thank M. M. Chowdhury for assistance with measuring the spectral response of the optical filter, E. Rahman for assistance with building the photodiode amplifier circuit, and H. D. E. Fan and M. Chang for the photo of the carbon nanotube forest. They acknowledge financial support from the Natural Sciences and Engineering Research Council of Canada (grant nos. SPG-P 478867, RGPIN-2017-04608, and RGPAS-2017-507958), the Canada Foundation for Innovation, and the British Columbia Knowledge Development Fund. This research was undertaken thanks, in part, to funding from the Canada First Research Excellence Fund, Quantum Materials and Future Technologies Program.

Conflict of Interest

The authors declare no conflict of interest.

Keywords

black body, carbon nanotubes, emissivity, graphene, thermal radiation

Received: October 28, 2019

Revised: January 1, 2020

Published online:

- [1] A. Nojeh, G. A. Sawatzky, L. A. Whitehead, *Appl. Opt.* **2019**, *58*, 2028.
- [2] A. Nojeh, *MRS Bull.* **2017**, *42*, 500.
- [3] F. Koppens, T. Mueller, P. Avouris, A. C. Ferrari, M. S. Vitiello, M. Polini, *Nat. Nanotechnol.* **2014**, *9*, 780.
- [4] D. K. Efetov, R. J. Shiue, Y. Gao, B. Skinner, E. D. Walsh, H. Choi, J. Hone, *Nat. Nanotechnol.* **2018**, *13*, 797.
- [5] S. Khasminkaya, F. Pyatkov, B. S. Flavel, W. H. Pernice, R. Krupke, *Adv. Mater.* **2014**, *26*, 3465.
- [6] Y. Yang, R. Zhao, T. Zhang, K. Zhao, P. Xiao, Y. Ma, P. M. Ajayan, G. Shi, Y. Chen, *ACS Nano* **2018**, *12*, 829.
- [7] H. Ghasemi, G. Ni, A. M. Marconnet, J. Loomis, S. Yerci, N. Miljkovic, G. Chen, *Nat. Commun.* **2014**, *5*, 4449.
- [8] C. N. Suryawanshi, C. T. Lin, *ACS Appl. Mater. Interfaces* **2009**, *1*, 1334.
- [9] Q. Ma, T. I. Andersen, N. L. Nair, N. M. Gabor, M. Massicotte, C. H. Lui, J. Kong, *Nat. Phys.* **2016**, *12*, 455.
- [10] M. Massicotte, P. Schmidt, F. Violla, K. Watanabe, T. Taniguchi, K. J. Tielrooij, F. H. Koppens, *Nat. Commun.* **2016**, *7*, 12174.
- [11] S. Tan, A. Argondizzo, C. Wang, X. Cui, H. Petek, *Phys. Rev. X* **2017**, *7*, 011004.
- [12] R. Bistrizter, A. H. MacDonald, *Phys. Rev. Lett.* **2009**, *102*, 206410.
- [13] V. Scardaci, Z. Sun, F. Wang, A. G. Rozhin, T. Hasan, F. Hennrich, A. C. Ferrari, *Adv. Mater.* **2008**, *20*, 4040.
- [14] Z. Sun, D. Popa, T. Hasan, F. Torrisi, F. Wang, E. J. Kelleher, A. C. Ferrari, *J. Nano Res.* **2010**, *3*, 653.

- [15] S. T. Huxtable, D. G. Cahill, S. Shenogin, L. Xue, R. Ozisik, P. Barone, P. Keblinski, *Nat. Mater.* **2003**, 2, 731.
- [16] Y. Miyoshi, Y. Fukazawa, Y. Y. Amasaka, R. Reckmann, T. Yokoi, K. Ishida, H. Maki, *Nat. Commun.* **2018**, 9, 1279.
- [17] T. Mori, Y. Yamauchi, S. Honda, H. Maki, *Nano Lett.* **2014**, 14, 3277.
- [18] J. Yan, M. H. Kim, J. A. Elle, A. B. Sushkov, G. S. Jenkins, H. W. Milchberg, H. D. Drew, *Nat. Nanotechnol.* **2012**, 7, 472.
- [19] J. M. Mitrani, M. N. Shneider, *Appl. Phys. Lett.* **2015**, 106, 043102.
- [20] R. Fainchtein, D. M. Brown, K. M. Siegrist, A. H. Monica, E. Hwang, S. D. Milner, C. C. Davis, *Phys. Rev. B* **2012**, 85, 125432.
- [21] L. M. Lawton, N. H. Mahlmeister, I. J. Luxmoore, G. R. Nash, *AIP Adv.* **2014**, 4, 087139.
- [22] N. H. Mahlmeister, L. M. Lawton, I. J. Luxmoore, G. R. Nash, *Appl. Phys. Express* **2015**, 9, 012105.
- [23] H. Zeng, C. Yang, J. Dai, X. Cui, *J. Phys. Chem. C* **2008**, 112, 4172.
- [24] Y. Wei, P. Liu, K. Jiang, S. Fan, *Nano Lett.* **2012**, 12, 2548.
- [25] P. Liu, L. Liu, Y. Wei, K. Liu, Z. Chen, K. Jiang, S. Fan, *Adv. Mater.* **2009**, 21, 3563.
- [26] M. Akoshima, K. Hata, D. N. Futaba, K. Mizuno, T. Baba, M. Yumura, *Jpn. J. Appl. Phys.* **2009**, 48, 05EC07.
- [27] P. G. Wiles, J. Abrahamson, *Carbon* **1978**, 16, 341.
- [28] R. Divigalpitiya, T. J. E. Clark, US Patent 8652375 B2, **2014**.
- [29] K. F. Mak, M. Y. Sfeir, Y. Wu, C. H. Lui, J. A. Misewich, T. F. Heinz, *Phys. Rev. Lett.* **2008**, 101, 196405.
- [30] E. Pop, V. Varshney, A. K. Roy, *MRS Bull.* **2012**, 37, 1273.
- [31] S. Cheon, K. D. Kihm, H. Kim, G. Lim, J. S. Park, J. S. Lee, *Sci. Rep.* **2015**, 4, 6364.
- [32] R. J. Thorn, O. C. Simpson, *J. App. Phys.* **1953**, 24, 633.
- [33] M. Chang, H. D. Fan, M. M. Chowdhury, G. A. Sawatzky, A. Nojeh, *Phys. Rev. B* **2018**, 98, 155422.
- [34] E. Pop, D. Mann, Q. Wang, K. Goodson, H. Dai, *Nano Lett.* **2006**, 6, 96.